LMU LUDWIG-MAXIMILIANS-UNIVERSITÄT MÜNCHEN

INSTITUT FÜR STATISTIK

Volker J Schmid

Spatio-Temporal Modeling of Perfusion Cardiovascular MRI

Technical Report Number 77, 2010
Department of Statistics
University of Munich

http://www.stat.uni-muenchen.de

Abstract

Myocardial perfusion MRI provides valuable insight into how coronary artery and microvascular diseases affect myocardial tissue. Stenosis in a coronary vessel leads to reduced maximum blood flow (MBF), but collaterals may secure the blood supply of the myocardium but with altered tracer kinetics. To date, quantitative analysis of myocardial perfusion MRI has only been performed on a local level, largely ignoring the contextual information inherent in different myocardial segments. This paper proposes to quantify the spatial dependencies between the local kinetics via a Hierarchical Bayesian Model (HBM). In the proposed framework, all local systems are modeled simultaneously along with their dependencies, thus allowing more robust context-driven estimation of local kinetics. Detailed validation on both simulated and patient data is provided.

1 Introduction

Contrast enhanced myocardial perfusion Magnetic Resonance Imaging (MRI) is a promising technique for providing insight into how reduced coronary flow affects the myocardial tissue. It also allows the understanding of microcirculation in the myocardial tissue and myocardial angiogenesis [1]. Clinically, myocardial perfusion MRI plays a major role in the evaluation of ischaemic heart disease beyond situations where there have already been gross myocardial damages such as acute infarction or scarring [2]. It is commonly used with drug-induced stress to identify tissue with restricted Myocardial Blood Flow (MBF) due to obstructive coronary lesions. Intra-coronary collaterals, *i.e.*, arteries and arterioles, which interconnect major coronary artery branches, can function as natural bypass vessels in the myocardium. In areas partially supplied by collaterals, the maximum blood flow may appear to be normal, but the arrival of contrast agent is delayed [3].

Analysis of myocardial perfusion MRI is typically performed via deconvolution of the myocardial signal response with an Arterial Input Function (AIF) measured in the blood pool, typically in the left ventricle. In the approach by Jerosch-Herold *et al.* [4], a penalty spline (P-Spline) is used to impose *a priori* smoothness constraints on the impulse response function in order to improve the numerical stability of the deconvolution process [5, 6]. The optimal value of the parameters can be determined using the L-curve method [7]. As an alternative method for estimating the smoothness of B-splines, Bayesian based frameworks have also been proposed [8]. As an advantage, Bayesian models allow adaptive, *i.e.*, time-varying smoothness parameters for the deconvolution process. For this reason, Bayesian

P-Spline models have received attention in both Dynamic contrast-enhanced MRI (DCE-MRI) [9] and myocardial perfusion MRI due to its flexibility in dealing with rapid changes in the response function [10].

To date, quantitative analysis of myocardial perfusion MRI has mainly been performed on data aggregated in pre-defined segment. A standardized definition of segments was given by the Cardiac Imaging Committee of the Council on Clinical Cardiology of the American Heart Association [11]. Analysis is done on segments rather than on voxels, as myocardial perfusion data has a low signal to noise ratio (SNR) which can be enhanced via aggregating over segments. However, by aggregating one loses the spatial and contextual information inherent in the images.

For analysis of collateral perfusion, contextual information can be important as it implicitly reflects the structure of microcirculation. Contextual information is frequently used in traditional image processing tasks, *e.g.* image de-noising or feature extraction. Two- and three-dimensional contextual information has also been used in medical image segmentation [12,13]. More recently spatial priors have been widely used in functional MRI [14–16], diffusion tensor imaging (DTI) [17] and DCE-MRI [18]. In these studies, the regression models in the "local" pixels are enhanced by contextual information from neighboring pixels using Markov random fields (MRF). MRFs are defined by specifying local neighborhoods, from which a global network of dependency is derived. A major challenge with this approach is to develop structural-preserving models, *i.e.*, models that do not smooth across structural boundaries or distinct features in the tissue. To this end, the set of neighbours have to be estimated adaptively from the data [8, 18]. Recently, spatio-temporal methods have attracted increasing attentions in medical image computing and the most challenging problems remain when spatial and temporal structures are not independent, but influenced by each other [19].

The purpose of this paper is to propose a spatio-temporal model for analyzing myocardial perfusion MRI. In normal myocardium, the blood flow in neighboring segments is largely similar. In the case of collateral flow under coronary obstruction, the response function is expected to be significantly different between segments. The focus of the proposed model is to quantify the dependencies between local kinetic systems. In the proposed framework, all local systems are modeled simultaneously along with their dependencies. It thus allows more robust context-driven estimation of local kinetics, a concept we call "contextual kinetics".

2 Theory and Methods

For modeling the signal intensity in the myocardial tissue, a Hierarchical Bayesian Model (HBM) is used. A HBM assumes the existence of unknown, latent variables, which cannot be observed [20]. In the context of myocardial perfusion, the spatial dependencies between different areas of the myocardium are such latent variables.

2.1 Local B-Spline model

In each voxel i, the observed signal intensity Y_{it} at time t is the unknown true signal intensity $S_i(t)$ plus an observation error ϵ_{it}. We assume a Gaussian observation error with unknown variance σ^2.

$$\epsilon_{it} \sim \mathrm{N}(0, \sigma_i^2) \text{ for all } i, t. \tag{1}$$

In the Bayesian framework, we use a relatively flat prior for the variance of the obsevation error, $\sigma^2 \sim \mathrm{IG}(a, b)$, with $a = 1, b = 10^{-3}$.

In general, the true signal intensity is the convolution of the arterial input function $A(t)$, *i.e.*, the signal intensity in the LV blood pool, and a response function $f(t)$ [1]

$$S_n(t) = \int_0^t A(t-u) f_n(u) du. \tag{2}$$

After discretization at time points $t_1, \ldots, t_T$,

$$S_{it_j} = \sum_{l=1}^{T} A(t_j - t_l) f_i(t_l) \Delta t = \sum_{l=1}^{T} A_{jl} f_i(t_l), \tag{3}$$

where Δt represents the sampling interval of the dynamic series and the matrix $\boldsymbol{A}$ is a convolution operator [4].

If we assume the response to be a smooth function, we can use a B-spline representation [4] for $f_i(t)$,

$$f_i(t_j) = \sum_{p=1}^{P} \beta_{ip} B_{pj}, \tag{4}$$

where $\boldsymbol{B}$ is a $T \times P$ design matrix of $4th$ order B-splines, and $\boldsymbol{\beta}_i$ represent the spline regression parameters for voxel i. In vector notation, Eqn. 3 and Eqn. 4 reduces to

$$\boldsymbol{S_i} = \boldsymbol{A f}_i = \boldsymbol{AB\beta}_i = \boldsymbol{D\beta}_i, \tag{5}$$

where $\boldsymbol{D} = \boldsymbol{AB}$ is the discrete convolution of the AIF with the B-Spline polynomials.

2.2 Temporal constraints

A typical constraint on $\boldsymbol{\beta}$ is a first or second order difference in the temporal dimension [4, 9]. In a Bayesian framework, this constraint is expressed as *a priori* distribution

$$\beta_{ip} \sim N\left(2\beta_{i,p-1} - \beta_{i,p-2}, \tau_p^2\right) \quad \text{for all } p = 1, \ldots, P-1 \tag{6}$$

This is also known as "random walk" prior [21], and the joint *a priori* distribution can be expressed as multivariate distribution

$$\boldsymbol{\beta}_{i\bullet} \sim N_P(0, \boldsymbol{R}^{-1}), \tag{7}$$

where N_P is the multivariate Gaussian distribution of dimension P, and $\boldsymbol{R}$ denotes the "precision matrix" (pseudo-inverse of a covariance matrix) of the random walk, including the temporal smoothness parameters τ_p^2, *cf.* [21]. As *a priori* distribution for the temporal smoothness parameters we use a Inverse Gamma distribution $\tau_p^2 \sim IG(c, d)$ with parameters $c = d = 1$, which implies a smooth, but flexible shape of the response function.

This model is similar to the model proposed by Jerosch-Herold *et al.* [4], however, formulated in a Bayesian framework. Estimates are identical whether the penalty is formulated as constraint as in [4] or as prior distribution as in Eqn. 6, *cf.* [22]. However, instead of first-order differences penalties used in [4] we use second-order differences, which implies smoother curves.

2.3 Spatio-temporal constraints

So far, the analysis is independent for each voxel. To account for the spatial structures of the image, we include contextual information and assume that spatially adjacent voxels share similar properties, *i.e.*, the shape of the response functions in neighboring voxels are similar. The shape of the response function is determined by the first order differences of the spline regression parameters. We therefore impose a stochastic constraint on the spline regression parameters,

$$\beta_{ip} \sim N\left(\frac{\sum_{j\sim i} \nu_{\{ij\}}\beta_j}{\sum_{j\sim i} \nu_{\{ij\}}}, \left(\sum_{j\sim i} \nu_{\{ij\}}\right)^{-1}\right) \quad \text{for each } i, p \tag{8}$$

where $i \sim j$ denotes that pixels segments i and j are adjacent. Due to the relatively large gaps between slices in myocardial perfusion MRI we discard neighbours in Z-dimension. Adjacent pixels are therefore defined by sharing a border in 2D, *i.e.*, we only use direct neighbourships. The spatial smoothing

parameter ν is defined for each pair $\{ij\}$ of adjacent pixels and describes the similarity between the shapes of the response functions in both pixels. For the spatial smoothing parameter, we use a Gamma prior distribution $\nu_{\{ij\}} \sim Ga(e, f)$ with $e = f = 1$.

The joint *a priori* distribution of the spatial constraint per knot p can be expressed by [23]

$$\boldsymbol{\beta}_{\bullet p} \sim N_N\left(0, \boldsymbol{Q}^{-1}\right), \tag{9}$$

where, $\boldsymbol{Q}$ is the precision matrix of a Markov random field (MRF) [24] incorporating the spatial distribution parameters $\nu_{\{nm\}}$. We combine the *a priori* constraints in Eqn. 7 and Eqn. 9 [23] in

$$\boldsymbol{\beta} \sim N_{N \cdot P}\left(0, (\boldsymbol{Q} \otimes \boldsymbol{S}) + (I_N \otimes \boldsymbol{R})^{-1}\right) \tag{10}$$

where $\boldsymbol{I}_N$ is the identity matrix with dimension $N \times N$.

2.4 Simulation study and *in vivo* data acquisition

For numerical validation, a set of myocardial perfusion images was simulated. To gain realistic simulations, we extracted response and input function from one scan from the *in-vivo* study below and, using these parameters, simulated signal voxel-wise from myocardial perfusion images. We used two simulation approaches: In simulation A, we smoothed the parameters derived from the in-vivo scans in order to suppress noise and simulated the signal per voxel. In simulation B, we applied standard segmentation and used the voxel with median MBF to simulate one signal for the whole segment. Afterwards noise was added per voxel. Fig. 1 shows true MBF values for both types of simulation.

In simulation A we assume that the MBF is spatially smooth, which is what the spatial approach proposes – so here we check whether the spatial approach can estimate spatial smooth MBF maps and what happens if we segment such data. In simulation B we use the assumption that the signal is identical in each voxel of a particular segment. Hence, we check whether the spatial approach can retain the borders between segments. White noise was added to the simulated signal per voxel to derive a signal-to-noise ratio per voxel of 3. Each simulation was repeated 50 times to evalute reliability of the proposed approach.

For *in-vivo* evaluation, MRI perfusion data from six patients with coronary artery disease was used [25]. The images were acquired with a 0.1 mmol/kg injection of a Gadolinium-based contrast agent on a 1.5-T Siemens Sonata scanner with single-shot FLASH with 48×64 pixel resolution on a 30×40 *cm* field of view (FOV) with a short saturation recovery time of 3.4

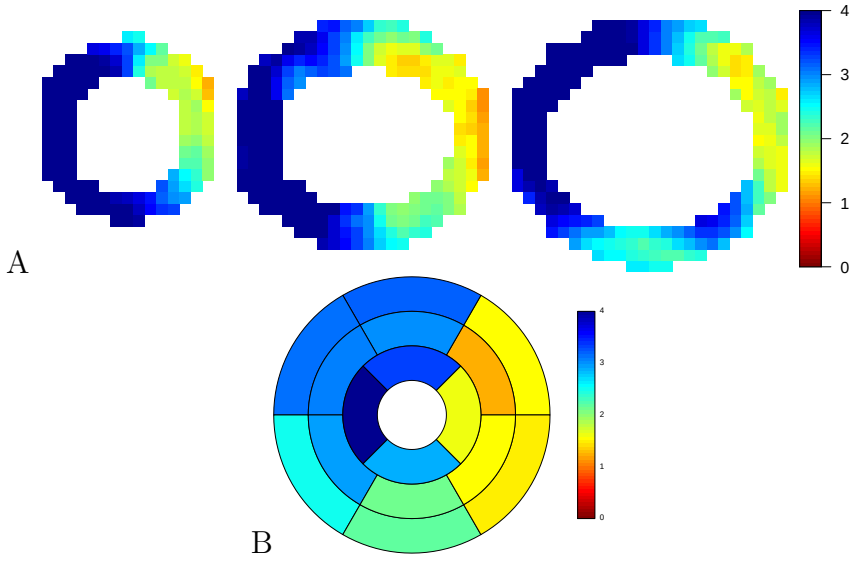

Figure 1: MBF values used in simulation

msec, TE= 0.5msec, TR= 1 msec for measurement of the LV blood pool, followed by measurement in the same cardiac cycles with a 108×256 pixel resolution on the same FOV with a longer saturation recovery time of 63.4 msec, TE = 1.2 msec, TR = 1.86 msec for measurement of the LV myocardium. Each subject was scanned once under rest, followed by a scan after injection of 140 μg/minute/kg of adenosine for four minutes, *i.e.*, under stress [1].

2.5 Bayesian results

For parameter estimation, we use a full Bayesian framework. That is, we draw conclusions only from the posterior probability density function (posterior pdf) $p(\theta|Y)$ with θ the vector of all unknown model parameter and Y the data, given by the Bayes formula

$$p(\theta|Y)\frac{\ell(Y|\theta)p(\theta)}{\int \ell(Y|\theta)p(\theta)d\theta} \tag{11}$$

where $\ell Y|\theta$ is the likelihood of the data given the model parameters, see Eqn. 1 and $p(\theta)$ is the prior pdf of the model parameters as specified in Eqns. 6 to 10.

Parameter inference is based on a Markov chain Monte Carlo (MCMC) algorithm [20]. The MCMC algorithm produces a random sample which

distribution is similar to the posterior pdf. From these samples, we can compute point estimates along with intervals to evaluate the uncertainty of the estimates. Here, we use the median of the sampled posterior pdf as point estimates and the quartile range (QR) of the computed sample in order to quantify the uncertainty of parameter estimation.

3 Results

3.1 Simulation study

To evaluate the simulation studies, we compare true and estimated maximum blood flow (MBF) derived with the approaches mentioned above. Table 1 lists bias, variance and mean squared error (MSE) between true MBF values and estimated values using the segmentation approach, the voxel wise approach and the proposed spatial approach. MSE can be decomposed in

$$MSE = Bias^2 + Variance.$$

For both simulations the MSE for the spatial approach is clearly smaller than the MSE of the segmentation and the voxel-wise approach. However, not only is the variance between true and estimated MBF values larger for segmentation approach and voxel-wise approach, there is also a noticeable bias, *i.e.*, MBF values are underestimated with voxel-wise and with segmentation approach. This is espacially true for segments and voxel with high (true) MBF, as we can see in the following figures.

Fig. 2 (a) depicts MBF values estimated using the segmentation approach for one of the per-voxel simulations. Naturally, this approach can depict

Table 1: Mean and standard deviation (in brackets) across sample of bias, variance and mean squared error between simulated and estimated MBF values for Simulation A (simulated voxel) and Simulation B (simulated segments)

Simulation A	Bias	Variance	MSE
voxel-wise	0.425 (0.0093)	0.359 (0.0255)	0.0528 (0.0139)
segment-wise	0.518 (0.0679)	0.237 (0.0560)	0.511 (0.0872)
spatial	0.071 (0.0148)	0.0481 (0.0032)	0.054 (0.0041)
Simulation B	Bias	Variance	MSE
voxel-wise	0.379 (0.0095)	0.497 (0.0232)	0.644 (0.0187)
segment-wise	0.549 (0.0647)	0.401 (0.0560)	0.712 (0.0757)
spatial	0.060 (0.0138)	0.018 (0.024)	0.022 (0.0027)

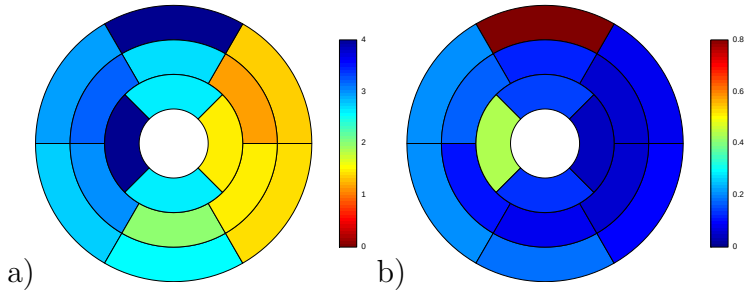

Figure 2: Left: Estimated MBF values for one run of the per-voxel-simulation A with segmentation approach in bulls eye representation. Right: QR of MBF estimation with segmentation approach for the same run.

the generally reduced MBF in the left circumflex artery (LCX). In the mid segment it also finds a reduced MBF in the right coronary artery (RCA), which is not visible in the true MBF values. Fig. 3 shows MBF values estimated using the proposed spatial approach. As we have seen from Table 1, estimated values are very similar to the true values. Local differences in MBF in a segment, for example in segment 5, are clearly restored. Fig. 4 depicts estimated values using a voxel-wise approach. As one can expect, the MBF "surface" is much more rougher compared to the spatial approach. Also we gain voxel-wise estimates, the localization of reduced microcirculation is much harder with this approach.

Fig. 2 (b) depicts the quantile range QR for the segmentation approach, Fig. 3 shows the QR for the spatial approach and Fig. 4 depicts the QR for the voxel-wise approach. Evidently, for segmentation approach and for voxel-wise approach the QR is dependent on the MBF values. In general, the QR is relatively low for both segmentation approach and spatial approach compared to the voxel-wise approach. This is due to the fact, that estimation in the voxel-wise approach is based on a lower amount of information, whereas the segmentation approach aggregates information in a segment and the spatial approach "borrows information" from neighbouring voxels. For the segmentation approach QR is only increased for a few segments with high MBF, hence the reliability for the segmentation and the spatial approach is similar.

Simulation B assumes that in each voxel of a particular segment the MBF is equal. Hence, the estimated MBF for the segmentation approach, shown in Fig. 7 is much more in accordance with the true values; this fact can also be seen in Table 1. Fig. 5 shows the estimated MBF values for the spatial approach. The segmental structure apparent in the simulated data is clearly

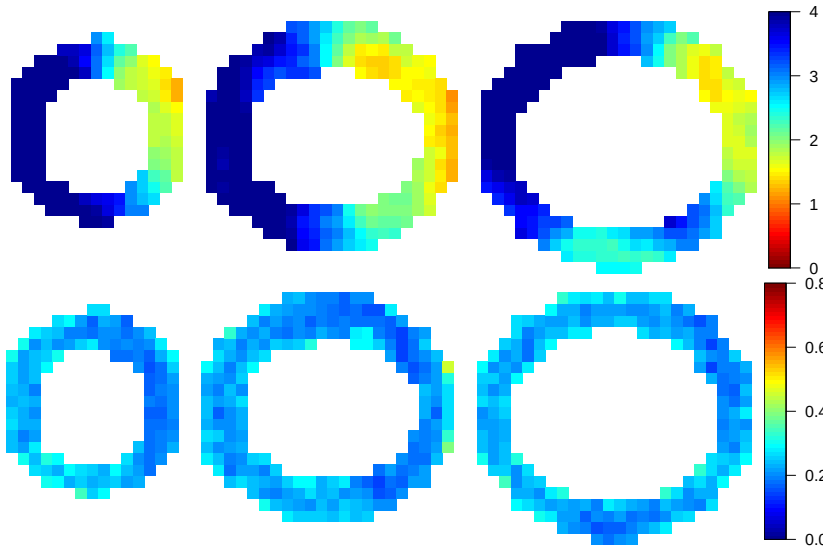

Figure 3: Top: MBF values for one run of the per-voxel-simulation A estimated with spatial approach. Bottom: QR of MBF estimation with spatial approach for the same run.

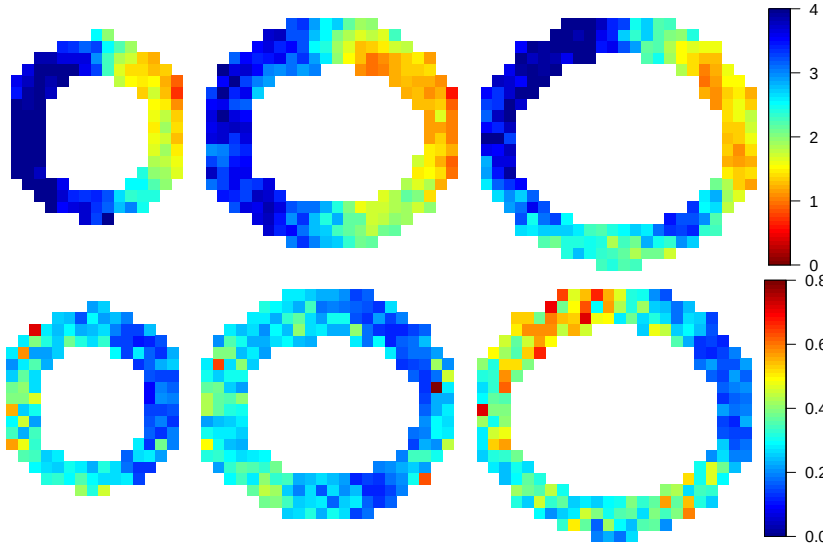

Figure 4: Top: MBF values for one run of the per-voxel-simulation A estimated with voxel-wise approach. Bottom: QR of MBF estimation with voxel-wise approach for the same run.

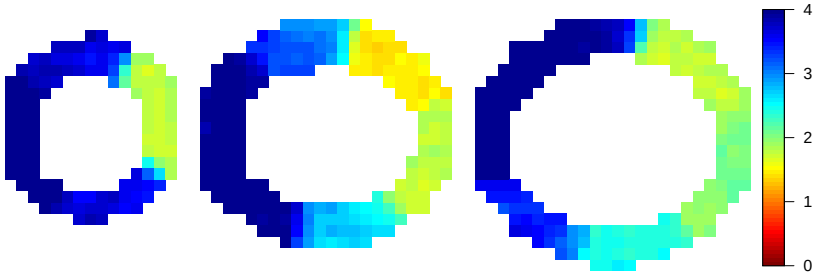

Figure 5: MBF values for one run of the per-segment-simulation B estimated with spatial approach.

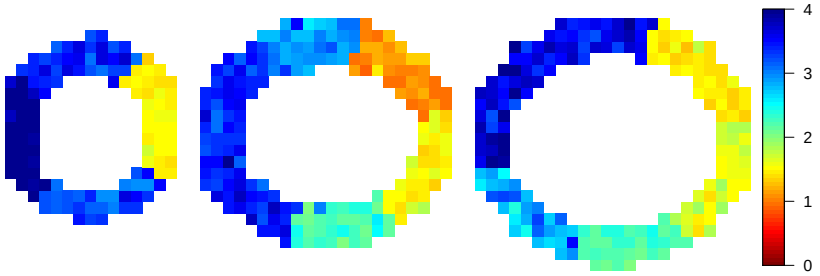

Figure 6: MBF values for one run of the per-segment-simulation B estimated with voxel-wise approach.

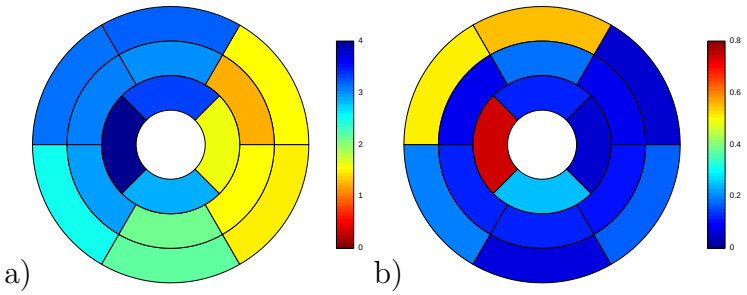

Figure 7: Left: Estimated MBF values for one run of the per-segment-simulation B with segmentation approach in bulls eye representation. Right: QR of MBF estimation with segmentation approach for the same run.

visible in this figure. However, for the voxel-wise approach depicted in Fig. 6 estimated values vary noticeable in each segment. Hence, by using spatial information we can retain the smooth structure of the MBF surface, however, due to the adaptive characteristics of the proposed approach, sharp feature – here the borders between segments – are retained.

In order to explore the causes for the under estimation of MBF values with the per segment approach, we take a look at the fits per voxel in segment 5 in one of the spatial simulations. Fig. 8 depicts simulated data along with fits from the spatial and the segmentation approach. Here, voxel in can basically be split into two cluster. Voxel in cluster 1 – depicted in black – have a fast upslope, whereas for voxel in cluster 2 – depicted in grey – the signal is dispersed, resulting in a lower MBF. Cluster 1 has a mean true MBF of 2.81 and cluster 2 has a mean true MBF of 1.68, resulting in a median true MBF for the whole segment of 2.05. The spatial approach gives a median MBF of 2.04 with two clusters of MBFs with means 2.71 and 1.64. For the segmentation approach, data are averaged in the segment. Fig. 8 shows the fit for the average signal in the segment. However, the average signal loses information as the fast upslope in cluster 1 is averaged out with the dispersion in cluster 2. Hence, the MBF is estimated as 1.50, even below the MBF of cluster 2.

3.2 *In-vivo* study

The proposed approaches were tested on six patients with different types of stenosis for clinical evaluation. Fig. 9 depicts estimated MBF values along with QR for the scans at rest and under stress for one of the patients using the segmentation approach. Fig. 10 depicts estimated MBF values along for with QR for the same scans with the spatial approach. In segment 1 and 6 both approaches show reduced blood flow at rest and under stress. Blood flow is also reduced at the apical slice, however, MBF values are typically lower with the segmentation approach compared to the spatial approach. In the mid slice at rest, the spatial approach picks up reduced MBF in segments 8 and 9, but the segmentation approach shows differences in MBF between these segments. However, the QR plots show that the estimates with the segmentation approach are rather unreliable here.

Table 2 lists the median difference between MBF values estimated with segmentation and spatial approach over all patients. In nearly all scans the estimates with the segmentation approach is considerable lower with the segmentation approach compared to the spatial approach. Table 2 also lists the median variance of MBF with the spatial approach per segment, *i.e.*, an estimate for the amount of variation of blood flow per segment. Typically this

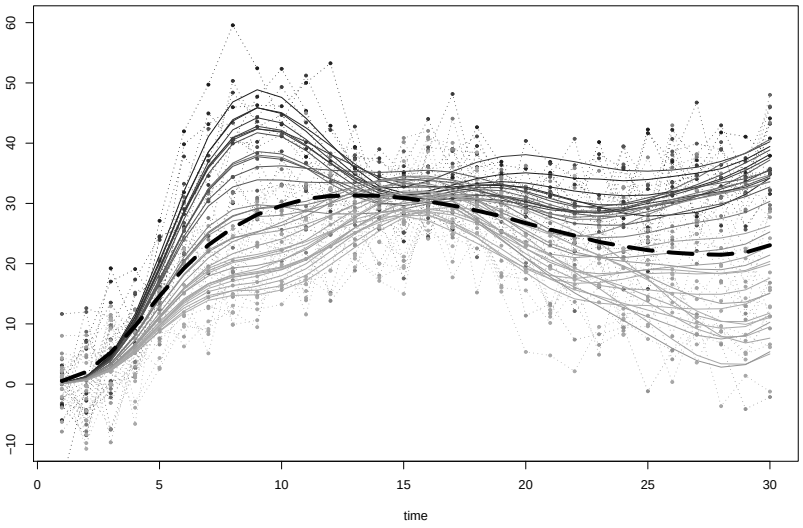

Figure 8: Simulated data (points) and fits with spatial approach (solid lines) in segment 5 of one run of simulation A. Fit with segmentation approach (dashed line). Data and fits are colored in grey and black according to true MBF.

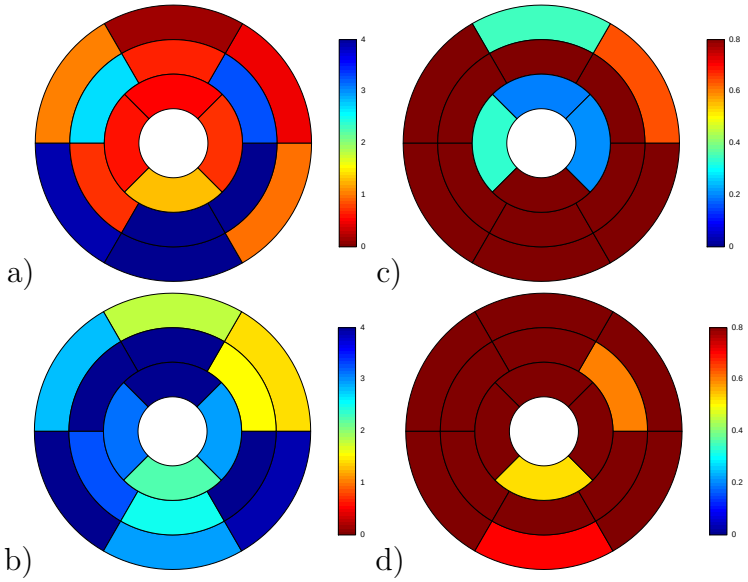

Figure 9: MBF for one patient estimated with segmentation approach. a) MBF at rest, b) QR of MBF at rest, c) MBF under stress, d) QR of MBF under stress.

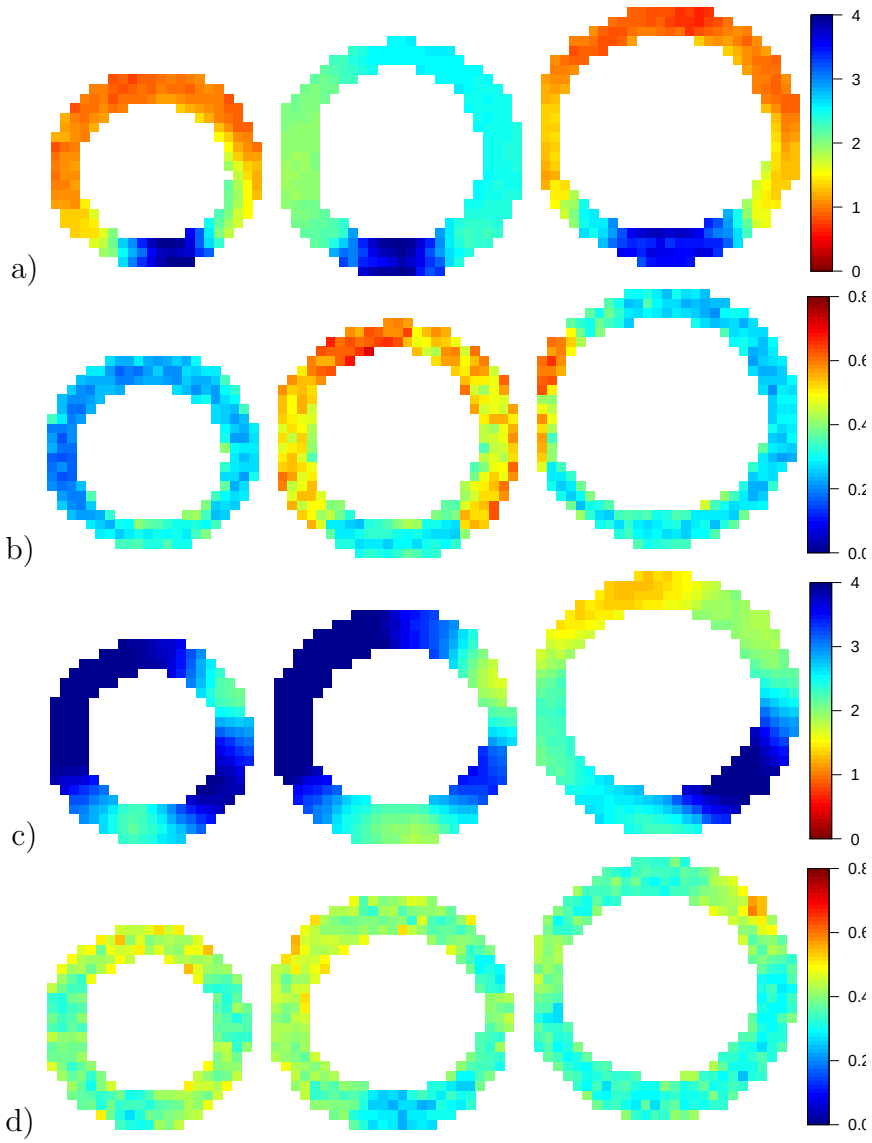

Figure 10: MBF for one patient estimated with spatial approach. a) MBF at rest, b) QR of MBF at rest, c) MBF under stress, d) QR of MBF under stress.

Table 2: Median and variance (in brackets) of differences between MBF values estimated with segmentation and spatial approach at rest and under stress for six patients in the *in-vivo* study

patient	1	2	3	4	5	6
at rest	0.497	0.305	0.242	0.448	0.740	0.933
	(0.098)	(0.038)	(0.023)	(0.080)	(0.030)	(0.008)
under stress	0.743	0.208	0.763	0.699	0.717	1.132
	(0.220)	(0.114)	(0.180)	(0.129)	(0.141)	(0.054)

number is higher for scans under stress due to higher values of MBF. In some patients, *e.g.* #6, the variation per segment is quite low, in others, *e.g.* #1, variation per segment is high, which indicates varying microcirculation per segment.

4 Discussion and Conclusion

In this paper, we have presented a spatio-temporal model for the analysis of myocardial first-pass perfusion MRI scans. The proposed model includes contextual information to describe the dependencies of the data in the individual segments. Validation with simulated data show that diseased areas can be detected by depicting the spatial distribution parameter between segments. By taking the complete shape of the response into account, the model highlights differences in delayed enhancement and altered kinetics. Differences in blood flow can result from reduced MBF, and hence stenosis in one of the segments, or from delayed arrival of tracer, hence due to the effect of collateral perfusion.

Simulation results indicate that by averaging the signal per segment, one not only loses information on local microcirculation, but also abets under estimation of blood flow. This is obviously even more important in cases where the blood flow varies in segments. When blood flow is identical over the segment, inaccurate segmentation may disturb the result. Small errors in the segmentation process can "contaminate" the average signal per segment and lead to wrong estimates. The spatial approach does not suffer from segmentation problems, even voxels which belong to the blood pool or to tissue surrounding the heart can be identified by the approach, as smoothing is locally adaptive. Local addictiveness is an important property of the proposed approach. It allows to retain sharp features and borders of the myocardial tissue and between segments.

Due to the high number of local smoothing parameters, the Bayesian ap-

proach, which estimates those "hyperparameters" along with other parameters, is more appropriate than an approach using penalties, which would require to choose the local smoothing parameters arbitrarily or via cross validation. However, the Bayesian approach has the disadvantage of long computation time. Estimation for a single slice can take up to an hour. As advantage, the Bayesian not only gives point estimates, but also information on the uncertainty of those estimates. In this paper, we used the quartile range of the posterior samples to evaluate the uncertainty.

In this paper, we only estimated the maximum blood flow (MBF) at rest and under stress. Many studies also look at the myocardial perfusion reserve (MPR). The MPR is given as MBF under stress divided through MBF at rest and, hence, can easily be computed from the results per segment. From the results of the spatial approach it is not as easy to compute the MPR. However, one can register scans at rest and under stress and, using the registration, compute the MPR. In summary, the proposed method provides additional information to the standard myocardial perfusion imaging analysis used in cardiovascular MRI, which can further enhance its clinical value.

Acknowledgements

Volker Schmid is supported by the LMUinnovative project BioMed-S: Analysis and Modelling of Complex Systems. *In-vivo* data were graciously provided by Peter Gatehouse, Cardiovascular Magnetic Resonance Unit, Royal Brompton Hospital, London, United Kingdom.

References

[1] M. Jerosch-Herold, R. T. Seethamraju, C. M. Swingen, N. M. Wilke, and A. E. Stillman, "Analysis of myocardial perfusion MRI," *J Magn Reson Imaging*, vol. 19, no. 6, pp. 758–70, 2004.

[2] J. R. Panting, P. D. Gatehouse, G.-Z. Yang, F. Grothues, D. N. Firmin, P. Collins, and D. J. Pennell, "Abnormal subendocardial perfusion in cardiac syndrome X detected by cardiovascular magnetic resonance imaging," *New England Journal of Medicine*, vol. 346, no. 25, pp. 1948–1953, 2002.

[3] M. Jerosch-Herold, X. Hu, N. S. Murthy, and R. T. Seethamraju, "Time delay for arrival of MR contrast agent in collateral-dependent

myocardium," *IEEE Trans Med Imaging*, vol. 23, no. 7, pp. 881–90, 2004.

[4] M. Jerosch-Herold, C. Swingen, and R. Seethamraju, "Myocardial blood flow quantification with MRI by model-independent deconvolution," *Medical Physics*, vol. 29, no. 5, pp. 886–897, 2002.

[5] P. Eilers and B. Marx, "Flexible smoothing with B-splines and penalties," *Statistical Science*, vol. 11, no. 2, pp. 89–121, 1996.

[6] B. Marx and P. Eilers, "Direct generalized additive modelling with penalized likelihood," *Computational Statistics and Data Analysis*, vol. 28, no. 2, pp. 193–209, 1998.

[7] P. R. Johnston and R. M. Gulrajani, "Selecting the corner in the L-curve approach to Tikhonov regularization," *IEEE Trans Biomed Eng*, vol. 47, no. 9, pp. 1293–6, 2000.

[8] A. Brezger, L. Fahrmeir, and A. Hennerfeind, "Adaptive Gaussian Markov random fields with applications in human brain mapping," *Journal of the Royal Statistical Society: Series C (Applied Statistics)*, vol. 56, no. 3, pp. 327–345, 2007.

[9] V. Schmid, B. Whitcher, A. Padhani, and G. Yang, "Quantitative analysis of dynamic contrast-enhanced MR images based on Bayesian P-splines," *IEEE Transactions on Medical Imaging*, vol. 28, pp. 789–798, 2009.

[10] V. J. Schmid, P. D. Gatehouse, and G. Z. Yang, "Attenuation resilient AIF estimation based on hierarchical Bayesian modelling for first pass myocardial perfusion MRI," in *Medical Imaging Computing and Computer-Assisted Intervention - MICCAI 2007*, vol. 10. Berlin: Springer, 2007, pp. 393–400.

[11] M. D. Cerqueira, N. J. Weissman, V. Dilsizian, A. K. Jacobs, S. Kaul, W. K. Laskey, D. J. Pennell, J. A. Rumberger, T. Ryan, and M. S. Verani, "Standardized myocardial segmentation and nomenclature for tomographic imaging of the heart. a statement for healthcare professionals from the cardiac imaging committee of the council on clinical cardiology of the american heart association," *Int J Cardiovasc Imaging*, vol. 18, no. 1, pp. 539–42, 2002.

[12] K. Held, E. Rota Kops, B. J. Krause, r. Wells, W. M., R. Kikinis, and H. W. Müller-Gartner, "Markov random field segmentation of brain MR images," *IEEE Trans Med Imaging*, vol. 16, no. 6, pp. 878–86, 1997.

[13] A. W. Liew and H. Yan, "An adaptive spatial fuzzy clustering algorithm for 3-d MR image segmentation," *IEEE Trans Med Imaging*, vol. 22, no. 9, pp. 1063–75, 2003.

[14] C. Gössl, L. Fahrmeir, and D. P. Auer, "Bayesian modelling of the hemodynamic response function in BOLD fMRI," *NeuroImage*, vol. 14, pp. 140–148, 2001.

[15] W. D. Penny, N. J. Trujillo-Barreto, and K. J. Friston, "Bayesian fMRI time series analysis with spatial priors," *NeuroImage*, vol. 24, no. 2, pp. 350–62, 2005.

[16] M. W. Woolrich, M. Jenkinson, J. M. Brady, and S. M. Smith, "Fully Bayesian spatio-temporal modelling of FMRI data," *IEEE Trans Med Imaging*, vol. 23, no. 2, pp. 213–31, 2004.

[17] S. Heim, L. Fahrmeir, P. H. C. Eilers, and B. D. Marx, "3D space-varying coefficient models with application to diffusion tensor imaging," *Computational Statistics & Data Analysis*, vol. 51, no. 12, pp. 6212–6228, 2007.

[18] V. J. Schmid, B. Whitcher, A. R. Padhani, N. J. Taylor, and G.-Z. Yang, "Bayesian methods for pharmacokinetic models in dynamic contrast-enhanced magnetic resonance imaging," *IEEE Transactions on Medical Imaging*, vol. 25, no. 12, pp. 1627–1636, 2006.

[19] L. Knorr-Held, "Bayesian modelling of inseparable space-time variation in disease risk," *Statistics in Medicine*, vol. 19, no. 17-18, pp. 2555–2567, 2000.

[20] W. R. Gilks, S. Richardson, and D. Spiegelhalter, *Markov Chain Monte Carlo in Practice*. London: Chapman & Hall, 1996.

[21] D. G. Clayton, "Generalized linear mixed models," pp. 275–301, 1996.

[22] L. Fahrmeir, T. Kneib, and S. Konrath, "Bayesian regularisation in structured additive regression: a unifying perspective on shrinkage, smoothing and predictor selection," *Statistics and Computing*, 2010, to appear.

[23] J. E. Besag and D. Higdon, "Bayesian analysis of agricultural field experiments," *Journal of the Royal Statistical Society Series B*, vol. 61, pp. 691–746, 1999.

[24] H. Rue and L. Held, *Gaussian Markov Random Fields: Theory and Applications*. Chapman & Hall/CRC, 2005.

[25] P. Gatehouse, A. Elkington, N. Ablitt, G.-Z. Yang, D. Pennell, and D. Firmin, "Accurate assesment of the arterial input function during high-dose myocardial perfusion cardiovascular magnetic resonance," *Journal of Magnetic Resonance Imaging*, vol. 20, pp. 39–45, 2004.